OPERATIONAL WINDOWS FOR DRY-WALL AND WETTED-WALL IFE CHAMBERS

F. NAJMABADI* *University of California, San Diego, Department of Electrical and Computer Engineering and Center for Energy Research, La Jolla, California 92093*

A. R. RAFFRAY *University of California, San Diego, Mechanical and Aerospace Engineering Department and Center for Energy Research, La Jolla, California 92093*

ARIES-IFE TEAM: S. I. ABDEL-KHALIK,† L. BROMBERG,‡ L. A. EL-GUEBALY,§ D. GOODIN,‖ D. HAYNES,§ J. LATKOWSKI,# W. MEIER,# R. MOORE,** S. NEFF,†† C. L. OLSON,‡‡ J. PERKINS,# D. PETTI,** R. PETZOLDT,‖ D. V. ROSE,§§ W. M. SHARP,# P. SHARPE,** M. S. TILLACK,‖‖ L. WAGANER,## D. R. WELCH,§§ M. YODA,† S. S. YU,†† M. ZAGHLOUL‖‖

Received May 3, 2004
Accepted for Publication June 15, 2004

The ARIES-IFE study was an integrated study of inertial fusion energy (IFE) chambers and chamber interfaces with the driver and target systems. Detailed analysis of various subsystems was performed parametrically to uncover key physics/technology uncertainties and to identify constraints imposed by each subsystem. In this paper, these constraints (e.g., target injection and tracking, thermal response of the first wall, and driver propagation and focusing) were combined to understand the trade-offs, to develop operational windows for chamber concepts, and to identify high-leverage research and development directions for IFE research. Some conclusions drawn in this paper are (a) the detailed characterization of the target yield and spectrum has a major impact on the chamber; (b) it is prudent to use a thin armor instead of a monolithic first wall for dry-wall concepts; (c) for dry-wall concepts with direct-drive targets, the most stringent constraint is imposed by target survival during the injection process; (d) for relatively low yield targets (<250 MJ), an operational window with no buffer gas may exist; (e) for dry-wall concepts with indirect-drive targets, a high buffer gas pressure would be necessary that may preclude propagation of the laser driver and require assisted pinch transport for the heavy-ion driver; and (f) generation and transport of aerosols in the chamber is the key feasibility issue for wetted-wall concepts.

KEYWORDS: *inertial fusion, fusion technology, IFE chambers*

*E-mail: najmabadi@fusion.ucsd.edu
†Georgia Institute of Technology, Woodruff School of Mechanical Engineering, Atlanta, Georgia 30332-0405
‡Massachusetts Institute of Technology, Cambridge, Massachusetts 02139
§University of Wisconsin, Fusion Technology Institute, Madison, Wisconsin 53706-1687
‖General Atomics, San Diego, California 92186
#Lawrence Livermore National Laboratory, Livermore, California 94550
**Idaho National Engineering and Environmental Laboratory, Fusion Safety Program, EROB E-3 MS 3815, Idaho Falls, Idaho 83415-3815
††Lawrence Berkeley National Laboratory, Berkeley, California 94720
‡‡Sandia National Laboratories, Albuquerque, New Mexico 87185
§§Mission Research Corporation, Albuquerque, New Mexico 87110
‖‖University of California, San Diego, Mechanical and Aerospace Engineering Department and Center for Energy Research, La Jolla, California 92093
##Boeing High Energy Systems, St. Louis, Missouri 63166

I. INTRODUCTION

The results from the ARIES-IFE study, an integrated investigation of inertial fusion energy (IFE) chambers and chamber interfaces with the driver and target systems, are discussed in this paper. The ARIES-IFE research was a national U.S. effort involving universities, national laboratories, and industry. As opposed to previous IFE power plant studies (e.g., Refs. 1 and 2), the ARIES-IFE research did not focus on developing a single design point. Rather, we performed detailed analysis of various subsystems parametrically to uncover key physics and technology uncertainties and to identify constraints imposed by each subsystem on the feasibility of IFE chamber concepts. The remaining papers in this special issue[3–8] describe the detailed analysis of the selected subsystem. The constraints from various subsystems were then combined in order to understand the trade-offs among subsystems, to develop operational windows for IFE chamber concepts, and to identify high-leverage research and development (R&D) directions for IFE research (the focus of this paper).

Many combinations of drivers (lasers, heavy ions, *Z*-pinch), targets (direct and indirect drive), and chamber concepts (dry wall, thin liquid protection, thick liquid walls) can be envisioned for an IFE power plant. An IFE power plant cycle starts with the explosion of the target in the chamber. The X rays, ions, and neutrons generated from the target explosion traverse the chamber, interact with the chamber constituents, and deposit their energy on the chamber wall. Clearly, the particle and energy loads on the wall will depend on the target yield and energy spectra as well as on the chamber constituents. The three classes of chamber concepts use different schemes to ensure survival of the first wall: gas protection for dry walls or liquid protection for the other two. In each case, the requirement for survival of the first wall leads to severe constraints on the chamber size and geometry, material choices, and maintenance of the chamber protection scheme (e.g., replenishment of the liquid protective layer). As a result of the interaction of the target particle and energy flux with the first wall, material is evaporated or ejected into the chamber. These materials evolve, cool, and are pumped out during the interval between driver shots. The chamber environment prior to the next shot will depend on the evolution of the chamber constituents during the time between shots. A cryogenic target has to be injected and tracked in this chamber, and the driver beams should be able to propagate and be focused in this preshot chamber environment. In our study, we have followed the above approach: We started from the target, found the response of the chamber to the target explosion, evaluated the chamber condition prior to the next shot, and studied whether targets can be successfully injected and ignited by the driver. This approach to a large extent has allowed us to decouple the driver design from the chamber performance. Study of target fabrication, injection, and tracking can also be done independently of other variations as they depend mainly on the target design and not on the chamber or driver concept. A major difference between previous U.S. IFE power plant studies[1,2] and ARIES-IFE research is the fact that detailed characterization of the IFE target yield and spectrum is now available. We will see that this detailed information of the target yield and spectrum plays a crucial role in defining the operational windows for IFE systems. We will also show that for dry-wall and thin-liquid-wall concepts, the blanket will experience a quasi-steady-state load comparable to that envisioned for magnetic fusion energy (MFE) power plants. As such, the first-wall protection system can be decoupled to a large degree from the blanket, and our research has focused on the wall protection scheme instead of the complete thermal power conversion system.

The plan for the paper follows this approach. In Sec. II, we review the reference targets used for the ARIES-IFE study. In Secs. III and IV, we explore the response of dry-wall and thin-liquid-protected (hereafter referred to as wetted-wall) chambers and the key critical issues for these chamber concepts. Much of the analysis on ablation and aerosol formation in thin-liquid-protected walls can also be extended to thick-liquid-wall concepts. In Sec. V, we explore target issues and derive the associated constraints on the chamber environment. In Sec. VI, we review the constraint imposed by driver propagation and focusing. Sections VII and VIII summarize the trade-offs, operational windows, and key uncertainties for the dry-wall and wetted-wall concepts. A summary and conclusions of our work are given in Sec. IX.

II. REFERENCE ARIES-IFE TARGETS

We have selected a heavy-ion indirect-drive target design from Lawrence Livermore National Laboratory/Lawrence Berkeley Laboratory[9] (LLNL/LBL) and a direct-drive target design from the Naval Research Laboratory[10] (NRL) as our reference targets. These targets were chosen because their construction and their output particle and energy spectra are vastly different. As a result, their manufacturing, injection, and tracking as well as the response of the chamber will be quite different and will allow a more thorough examination of R&D issues.

The cross section of the 154-MJ NRL direct-drive target[10] as well as the driver power profile is shown in Fig. 1. This target achieves a gain of 120. In addition to this target, a higher-yield direct-drive target (400 MJ) was also considered in some of the ARIES-IFE analyses[3,4] to explore the impact of the yield on the power plant operational windows. The energy spectrum and energy partitioning of this higher-yield target, however, are similar to the 154-MJ version.

The cross section of the 458-MJ heavy-ion indirect-drive target from LLNL/LBL (Ref. 9) is shown in Fig. 2.

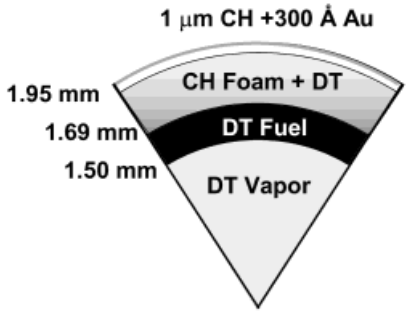

Fig. 1. Cross section of the 154-MJ NRL direct-drive target.[10]

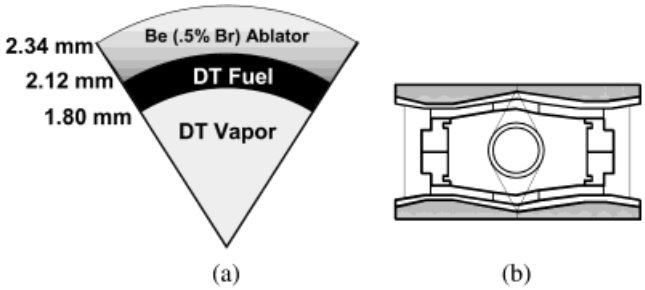

Fig. 2. Cross section of 458-MJ LLNL/LBL distributed radiator indirect-drive target.[9] The capsule (a) is located inside a radiation hohlraum (b).

This target utilizes a radiation hohlraum enclosure and has a gain of 140. The X rays resulting from the driver beam interaction with the hohlraum material are then deposited on the deuterium-tritium (D-T) capsule inside the hohlraum and would ignite the capsule. The detailed spectra of the target emissions for both targets have been calculated.[11] While the reference indirect-drive target is optimized for a heavy-ion driver, the target emission spectra and energy partitioning would be qualitatively similar to those of a laser-driven indirect-drive target.

The breakdown of energy partitioning in different channels for both targets is given in Table I. Data in Table I show that ~70% of the target yield is carried by neutrons for both targets. These neutrons pass through the first wall and deposit most of their energy in the blanket and, therefore, do not pose a major thermal threat to the first wall. The remaining ~30% of target energy, however, appears as surface heat flux or near-surface heating in the first wall. There is a major difference between the two targets in this regard. In the indirect-drive target, the ions slow down in the high-Z hohlraum material, and their energy is converted into soft X rays (<1 keV). As such, ~25% of the target yield appears as X rays and only ~6% as ion kinetic energy. In the direct-drive target (no high-Z hohlraum), ions maintain their energy, and only a small fraction of energy appears as X rays (mainly from bremsstrahlung emitted by the fusion plasma).

The ions and X rays are generated in the explosion target in a subnanosecond timescale. However, the energy flux at the chamber wall depends on the time it takes photons and ions to traverse the chamber. As all photons travel with the same speed, the X-ray pulse on the first wall has the same duration as that emitted from the target (subnanoseconds). As such, if a large portion of the target yield is released as X rays (as in the indirect-drive target above), the heat flux on the wall can become too high, and a "bare" solid wall cannot accommodate such an X-ray threat. The burn products (fast ions) and debris ions, however, are emitted with a wide range of kinetic energy (and speed). These ions arrive at the first wall at vastly different times (see Fig. 3). This difference in the time-of-flight will spread the initial subnanosecond burst of ions into a longer microsecond-pulse arriving at the wall, leading to a much lower heat generation rate in the first wall. This time-of-flight spreading of ion energy flux was not included in previous IFE power plant studies

TABLE I

Energy Partitioning of the Target Designs Used in the ARIES-IFE Study

	NRL Direct-Drive Target		Heavy-Ion Indirect-Drive Target	
	Energy (MJ)	Fraction of Total Yield (%)	Energy (MJ)	Fraction of Total Yield (%)
Driver energy	1.3		3.3	
Total yield	154		458	
Neutrons	109	71	316	69
Burn product fast ions	19.5	13	8.43	1.8
Debris ion kinetic energy	22.1	14	18.1	4.0
X rays	2.1	1.4	115	25

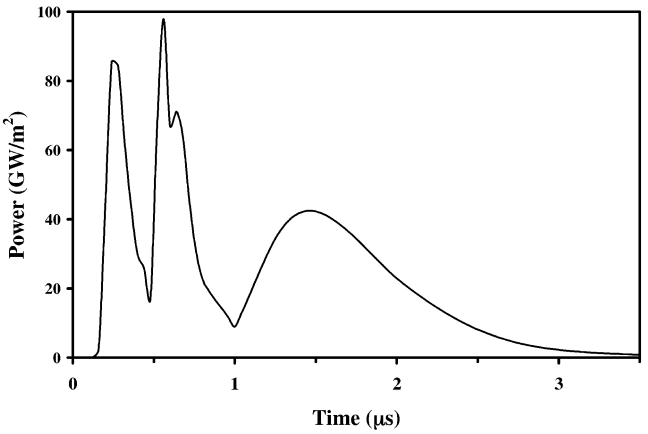

Fig. 3. Temporal profile of ion power arrived at the wall of a 6.5-m-radius chamber (based on 154-MJ NRL emission spectra). The time of flight of ions has spread the initial subnanosecond pulse to several microseconds. The three distinct power pulses are due to (from left to right) fast D-T, fast helium, and debris ions (deuterium/tritium/helium).

(e.g., Refs. 1, 2, and 12). It was demonstrated at the initial phase of the ARIES-IFE study that the time-of-flight spreading of the ion energy flux together with the lower X-ray output of the modern direct-drive targets could allow "bare" solid walls to accommodate the heat flux from direct-drive targets.[13] The impact of time-of-flight spreading of ion energy on the performance of wetted-wall chambers was also investigated recently in an update of the Koyo study.[14]

III. DRY-WALL CHAMBER CONCEPTS

III.A. Buffer Gas

Dry-wall chambers are desirable because of their relative simplicity. An IFE power plant will probably operate with a repetition rate of 5 to 15 Hz ($\sim 3 \times 10^8$ shots/yr). Thus, even a nanometer ablation of the first wall during a single IFE shot will lead to an unacceptably low wall lifetime. Previous IFE power plant studies[1,2,12] had assumed target emission and spectra similar to those of the indirect-drive target of Table I; i.e., a large portion of target yield is emitted as soft X rays. As such, these studies had predicted a very large heat flux on the first wall and concluded that a "bare" solid wall cannot survive IFE power plant conditions. The Solase study[12] had proposed the use of a high-Z protective or buffer gas for dry-wall concepts. The high-Z gas would absorb the X-ray energy from the target and reradiate the energy. With sufficient gas density, the radiation transport in this buffer gas would increase the duration of the X-ray pulse from subnanoseconds to several microseconds and reduce the heat load to a level such that the ablation of the first wall by the thermal load (i.e., evaporation) would not occur. Detailed radiation transport analysis in the Sombrero[1] study had led to the conclusion that ~5 torr of xenon is needed for this purpose. However, this level of buffer gas density will have a major impact on the propagation and focusing of driver beams as well as on the survivability of the targets during the injection process. These trade-offs are discussed in Secs. V and VI. (While the number density of the buffer gas is the correct parameter, the pressure of the cover gas is quoted throughout this paper for convenience. The pressure is calculated assuming room temperature conditions: 1 mtorr $\approx 3.5 \times 10^{19}$ atoms/m^3.)

III.B. Use of Armor

The energy threat to the first wall is due to high-energy ions and X-ray photons. Photon and ion energy depositions fall by one to two orders of magnitude within the first 100 μm of the first wall. Our analysis, below, indicates that beyond this 100- to 200-μm region, the first wall experiences a much more uniform, quasi-steady-state heat flux with values similar to those in MFE devices. As such, it is prudent to use a thin armor instead of a monolithic first wall. The armor can then be optimized to handle the highly transient particle and heat fluxes while protecting the first wall. The first wall can then be optimized for structural function and efficient heat removal at quasi-steady-state. IFE armor conditions are similar to those for plasma-facing components in MFE devices as is shown in Table II. As such, the large body of research performed for MFE plasma-facing components can be utilized in developing IFE armors. Furthermore, as most of the neutrons are deposited in the back where the blanket and coolant temperatures will be at quasi steady state because of the thermal capacity effect, most first-wall and blanket concepts developed for MFE will be directly applicable to IFE applications.

III.C. Armor Material

The armor material must have high-temperature capability and excellent thermophysical properties to accommodate the high incident energy flux. There are several possibilities for armor material: (a) tungsten and refractories, (b) carbon [and carbon-fiber composites (CFCs)], and (c) more exotic engineered materials (such as a high-porosity fibrous carpet).[3] Each has its own set of potential advantages and critical issues that should be addressed with rigorous R&D. Carbon and CFC composites are widely used in plasma-facing components in present MFE experiments. However, carbon suffers from several other mass loss processes such as chemical erosion and radiation-enhanced sublimation. Codeposition of sublimated carbon with tritium is also a major safety concern for fusion systems. Tungsten and other refractories alleviate these concerns. However, melting and stability of

TABLE II

A Comparison of Estimated Thermal Threats on Typical IFE Armor (Direct-Drive NRL Target[10]) and ITER Plasma-Facing Components by Edge-Localized Modes, Vertical Displacement Events, and Disruptions

	ITER Type-I Edge-Localized Mode	ITER Vertical Displacement Event	ITER Disruption	Typical IFE Armor
Energy	<1 MJ/m^2	$\sim$50 MJ/m^2	$\sim$10 MJ/m^2	$\sim$0.1 MJ/m^2
Time	100 to 1000 μs	$\sim$0.3 s	$\sim$1 ms	1 to 3 μs
Frequency	Few hertz	$\sim$1/100 discharges	$\sim$1/10 discharges	5 to 15 Hz
Base temperature	200 to 1000°C	$\sim$100°C	$\sim$100°C	$\geq$500°C

the melt layer as well as exfoliation of tungsten under large helium ion fluxes requires extensive R&D. The acceptable lifetime for the bond between the armor and the first wall under cyclic load conditions should also be demonstrated.

III.D. Thermal Response of the Armor with Direct-Drive Targets

As the pressure of the buffer gas has a major impact on target injection and tracking as well as on propagation and focusing of the driver beams, the thermal response of the armor was first calculated in the presence of *no* buffer gas. Results of this analysis are discussed in detail in Ref. 3. Figure 4 shows the thermal response of a 3-mm tungsten armor to the threat spectra from the 154-MJ NRL direct-drive target for a 6.5-m-radius chamber. The armor was assumed to be cooled by 500°C helium gas. The temporal profiles of the tungsten armor temperature at different depths from the surface are shown. It can be seen that the maximum temperature of the tungsten armor is $\sim$2900°C, which is well below the melting point of tungsten (3410°C), and this armor can handle the energy load.

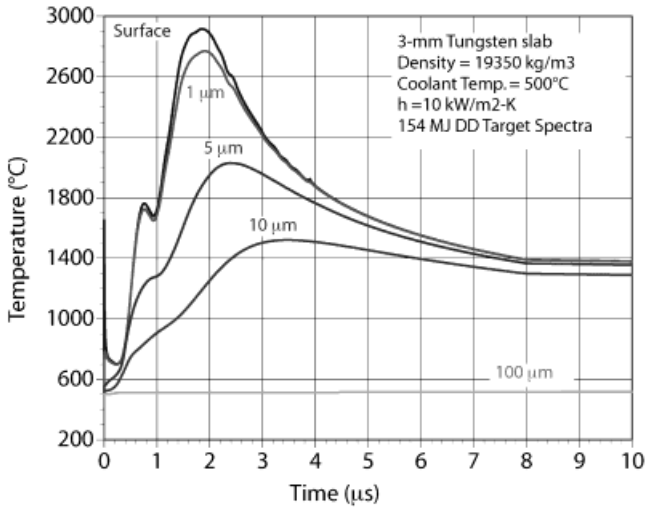

Fig. 4. Thermal response of a 3-mm tungsten armor to the NRL direct-drive target in a 6.5-m-radius chamber with no protective gas. Temporal profiles of temperature at different depths of the armor are shown. At depths >100 μm, the armor/first walls experience a quasi-steady-state heat flux.

The temporal variation of the armor surface temperature clearly shows three peaks corresponding to the arrival of X rays (an 1150°C temperature spike overlaid on the vertical axis), fast ions (at $\sim$0.8 μs), and slow debris ions (at $\sim$2 μs). It is important to note that the maximum temperature of the armor occurs during the slow/debris ion energy pulse and is not due to the X-ray pulse. These three peaks almost disappear 10 μm into the armor. At this depth, the armor is heated more or less uniformly in 3 μs and then cools slowly ($\sim$10 ms) back to its original $\sim$500°C equilibrium temperature. At depths >100 μm, the armor experiences a quasi-steady-state heat flux. Similar analysis performed for carbon shows a peak surface temperature of 1900°C and a negligible sublimation rate of <1 μm/yr. Based on these results and on the assumption of an armor temperature limit based on the melting point for tungsten and on minimal sublimation for carbon, it appears that no buffer gas is necessary to protect the armor from the thermal energy of a 154-MJ NRL direct-drive target for the assumed chamber size. Even higher yields (up to $\sim$250 MJ) could be accommodated under these criteria. However, for much higher yields, some form of gas protection will be necessary for similar chamber sizes (e.g., $\sim$60 mtorr of xenon for a 400-MJ target), and/or chamber size should be increased. The buffer gas, in this case, absorbs some slow/debris ion power through atomic collisions, thereby reducing the maximum armor temperature to an acceptable level. The exact value of the target yield at which the gas protection becomes necessary depends on the evolution of the target energy and the threat spectra as the yield is increased.

Note that the above conclusions are based on the assumption that the armor temperature is limited by avoidance of melting for tungsten and by achieving minimal sublimation for carbon. It is possible that other mechanisms affecting the armor lifetime would be triggered at

a lower armor temperature (e.g., cracks induced by thermal stress). Separately, the above results are calculated for an ideally flat and monolithic armor and show that most thermal transients occur within a depth of 10 to 20 μm. The surface morphology of the IFE chamber armor will probably have features >100 μm. Impurities in the armor can cause local hot spots (because of different penetration depths of photons and ions). As such, the above conclusions should be confirmed with further R&D and especially experimentation.

III.E. Thermal Response of the Armor with Indirect-Drive Targets

Because of the large energy content in the X-ray channel, dry-wall chambers require a buffer gas to be able to withstand the indirect-drive target explosion. BUCKY, a one-dimensional Lagrangian radiative-hydrodynamics code,[15] is used for the simulation of the response of the buffer gas and armor to target X-ray and ion threat spectra. Calculations were performed for different equilibrium xenon densities and wall temperatures. Figure 5 shows the results for a 6.5-m-radius chamber with a graphite wall. In this case, the maximum wall temperature for which negligible ablation of carbon armor occurs is plotted as a function of the required xenon buffer gas density (1 mtorr xenon at room temperature $\approx 3.5 \times 10^{19}$ atom/m^3). This figure represents the operational window for the chamber thermal response; the area below the curve is the acceptable region of operation. The amount of xenon required to prevent an unacceptable mass loss per shot depends on the yield of the target as well as on the partitioning and spectra of the X rays and ions. This is also illustrated in Fig. 5 as the design for the 154-MJ NRL direct-drive target as well as a "scaled" 400-MJ direct-drive target is plotted. It is clear that the indirect-drive targets with a larger energy in the X-ray channel require a considerably higher density of the buffer gas.

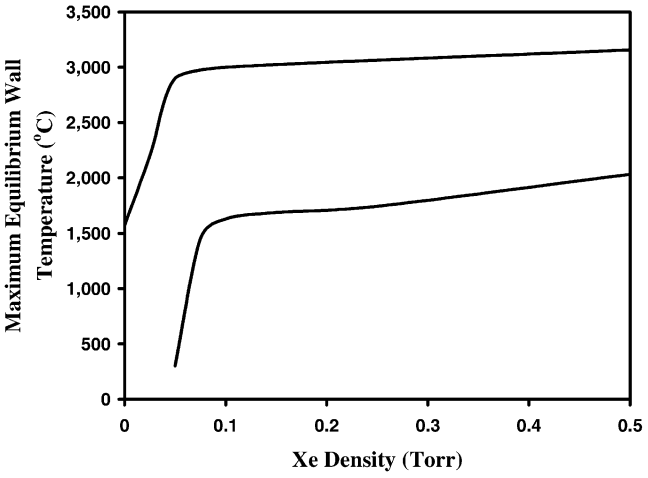

Fig. 5. Maximum wall temperature for which a negligible ablation of carbon armor occurs as a function of the required xenon buffer gas density (1 mtorr xenon at room temperature $\approx 3.5 \times 10^{19}$ atoms/m^3) for three different targets. The area below each curve represents the thermal operational window of the IFE chambers to that target.

IV. WETTED-WALL CHAMBER CONCEPTS

The wetted-wall (or thin-liquid-protected wall) combines the attractive features of a solid wall (robust mechanical design and efficient energy recovery) with the advantages of a renewable armor to accommodate the X-ray and ion threats produced by IFE target explosions. Renewability of the liquid-film armor removes the near-zero ablation threshold of the solid wall. On the other hand, part of the liquid-film armor evaporates under the incident X-ray and ion energy fluxes and enters the chamber in each shot. As such, the key feasibility issues for this concept are (a) reestablishment of the liquid-film armor between shots (as part of the liquid has been evaporated) and (b) reestablishment of a quiescent chamber environment prior to the next shot as evaporated liquid armor material has entered the chamber and should be removed. In the latter case, generation and transport of aerosols in the chamber is a key issue in arriving at an acceptable condition for the injection of new targets and propagation of driver beams.

IV.A. Film Dynamics

As part of the ARIES-IFE study, experimental and numerical studies have been conducted to examine the fluid dynamic aspects of liquid-film protection systems with either radial injection through a porous first wall or forced flow of a thin liquid film tangential to a solid first wall.[4,5] For both the radial injection and forced film designs, our efforts have been focused on examining the behavior of the liquid film on the downward-facing surfaces (upper section) of the IFE chamber, where virtually no work has been done before. Among the critical questions needed to establish the viability of the wetted-wall concept are the following:

1. Can a stable liquid film be maintained on the upper section of the chamber? (That is, how long does it take before the liquid "drips" into the chamber?)

2. Can the film be reestablished over the entire chamber surface prior to the next target explosion?

3. Can a minimum film thickness be maintained to prevent dry patch formation and provide adequate protection during the next target explosion?

For the radial injection scheme, generalized nondimensional charts for the droplet detachment time as a function of the initial thickness, injection velocity, Reynolds number, and surface mass flux have been developed.[5,16] These results suggest that liquid film stability may impose a limit on the minimum repetition rate in order to avoid liquid "dripping" into the chamber between shots. Generalized charts have also been developed for the minimum film thickness during the evolution of the free surface prior to droplet detachment and the equivalent diameter of the detached droplets as functions of the initial film thickness, injection velocity, Reynolds number, and nondimensional mass flux at the interface (due to condensation or evaporation).[5,16] These results suggest that a minimum injection velocity will be required to prevent the film thickness from decreasing below a designer-specified minimum value dictated by wall protection requirements. A preliminary experimental investigation aimed at validating the model has been performed; the data show good agreement with model predictions.

For the forced-flow scheme, an experimental study[5,17] has been performed to determine the effect of various design and operational parameters on the film detachment distance downstream of the introduction point for downward-facing flat surfaces with various inclination angles. Generalized nondimensional charts of the film detachment distance normalized by the initial film thickness as a function of the Froude number for both wetting (glass) and nonwetting (Rain-X coated glass) fluids were generated. The data suggest that the normalized detachment distance strongly depends on the Froude number and surface characteristics (i.e., wettability). These data allow the designers to establish the maximum allowable spacing between film injection and liquid return points along the chamber surface to avoid film detachment. Experiments have also been performed to examine the behavior of liquid films flowing around cylindrical obstacles, typical of the protective dam shielding beam and target injection ports.[5,17] These results indicate that the presence of such obstacles will pose a significant challenge to the designers, inasmuch as the disrupted film may directly interfere with the intended function of the port (e.g., beam propagation or target injection).

In summary, the radial injection scheme appears to be feasible and does not impose major constraints on the feasibility of wetted-wall concepts. The attractiveness of this scheme, to a large degree, depends on the details of the chamber and power plant design and the impact of the required pumping power on the overall recirculating power and economics of the power plant. For the forced-flow scheme, the behavior of the film near major obstacles is a major concern and requires further R&D.

IV.B. Thermal Response

As a result of the energy delivered from the IFE target explosion, a part of the liquid protection of the first wall is ablated in each shot and enters the chamber. The magnitude of the heating rate dictates the dominant boiling process: surface evaporation, heterogeneous nucleation, and/or homogeneous nucleation. In the case of ions from the IFE target, the heating rates are small enough such that the main boiling process is surface evaporation and the ablated material enters the chamber as vapor. The heating rate by X rays is, however, so large that neither surface evaporation nor heterogeneous nucleation plays a major role; i.e., the heating rate is so high that the surface evaporation process does not have sufficient time to occur.[4] Instead, for such extremely high heating rates, the boiling process is dominated by homogeneous nucleation, which leads to "explosive boiling." This involves rapid superheating to a metastable liquid state with large excess free energy, which decomposes explosively into liquid and vapor phases. As a result, the amount of ablated material would be much larger than would be estimated through the energy balance between the incident energy and the phase change alone—a large fraction of protective liquid may enter the chamber as liquid droplets.[4] Figure 6 shows the region in which explosive boiling can occur in a chamber protected by a lead film subjected to the X-ray flux from the 458-MJ indirect-drive target. Substantial experimental and theoretical research is needed to accurately estimate the amount of material that will enter the chamber through explosive boiling; Fig. 6, however, can be used to determine the upper bound.

A lower bound for the amount of material that is ablated and introduced into the chamber can be found by ignoring explosive boiling and splashing. BUCKY simulations were performed for a 4.5-m-radius chamber, initially filled with 1 mtorr lead and protected by a 1-mm

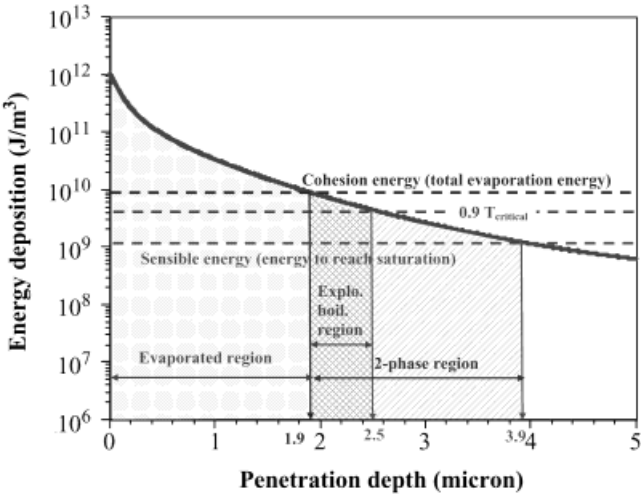

Fig. 6. Volumetric heat deposition in a lead film from 458-MJ indirect-drive X-ray spectra illustrating two-phase region and regions where explosive boiling is likely to occur.

lead film. Simulations for the 458-MJ indirect-drive target showed that a total of 21.4 kg of lead will be evaporated in each shot. Of the 22 MJ of energy in target ions, only 5.3 MJ is deposited in the liquid as opposed to the vapor, with none penetrating farther than ~0.65 mm into the liquid. Simulations for the 154-MJ direct-drive target resulted in evaporation of 9.2 kg/shot of lead.

IV.C. Chamber Clearing

The material ablated from the protective film should be removed from the chamber before the next shot can be initiated. Previous studies had usually assumed that the material induced in the chamber is only in the vapor form (ignoring explosive-phase boiling and splashing), which underestimates the source term. In addition, it was usually assumed that the vapor in the chamber will condense on the wall surface, which ignores generation of aerosol in the chamber. Following this assumption, one finds for the BUCKY simulation of the 458-MJ indirect-drive target above that the initial lead density of 1 mtorr can be reestablished within 0.15 s of the IFE shot—a repetition rate of 5 Hz is possible for this configuration.

Our analysis of aerosol generation and transport in the IFE chambers indicates that aerosol and not the vapor will dominate the chamber clearing process.[5] For example, for a 6.5-m-radius chamber protected by 1 mm of flibe, exposure to the 458-MJ indirect-drive target will lead to ablation of ~5.5 μm of flibe (if explosive boiling is ignored), and ~5.7 kg of flibe enters the chamber. We find that after ~1 ms, 3.5 kg of flibe will be in the form of aerosol and remains so afterward. Only the aerosol sizes and distribution evolve afterward, and at 0.25 s, there are still ~10^9 to 10^{10} aerosol droplets/m^3 dispersed throughout the chamber volume with sizes of ~0.5 to 5 μm. There are many uncertainties in the analysis of aerosol generation and transport in the IFE chambers such as the coagulation and reflection behavior of droplets of different sizes and velocities impacting a liquid wall (aerosol transport) as well as ion-enhanced nucleation (aerosol generation). Droplets entering the chamber through explosive boiling should also be considered. Overall, aerosol generation and transport is the critical feasibility issue for wetted-wall concepts. This is also a critical feasibility issue for thick-liquid-wall chambers.

V. TARGETS

The direct-drive IFE targets include spherical layers of frozen D-T (at ~18 K) encapsulated in layers of foam or plastic. The target should have a high degree of spherical symmetry and surface smoothness. The indirect-drive targets include a capsule (which is very similar to the direct-drive target) that is suspended in a hohlraum. Fabrication of these targets at a rate required for a power plant (~500 000/day) and an acceptable cost remains a feasibility issue for IFE, and R&D on cost-effective means for their mass production is ongoing.[18,19] Once produced, these targets should be injected into an IFE chamber with sufficient velocity (50 to 400 m/s) and placed within several millimeters of the chamber center (where the driver beams are focused). Gas-gun target injectors are under development.[20]

V.A. Target Survival During Injection

Inertial fusion targets should maintain their high degree of spherical smoothness and symmetry during the injection process. In particular, targets can heat up during the travel in the chamber by friction (energy exchange from the chamber constituents) as well as by radiation heating from the hot walls of a power-producing chamber. These cryogenic targets are produced through careful layering at 18 K in order to achieve the required degree of spherical smoothness. To date, attempts to lower the temperature of the target after fabrication to allow for a larger margin for heating during the injection process have failed. As such, we have assumed that the target is 18 K at the time of injection into the chamber. Although the maximum temperature limit to prevent unacceptable target outer layer deformation is not well known, the previous assumption was to maintain the target D-T temperature below its triple point, 19.8 K (Ref. 21).

For indirect-drive targets, the fragile cryogenic capsule is surrounded by a relatively massive hohlraum that insulates it from the heat load during the transit to the center of the chamber. Therefore, the cryogenic capsule will effectively remain at 18 K during injection over a wide range of operating conditions.

Direct-drive targets do not have such insulation, and their heating during injection is of particular concern since it could lead to unacceptable target deformation and/or density variations. The thermal response of the 154-MJ direct-drive target (Fig. 1) was determined parametrically assuming a two-dimensional (2-D) heat flux distribution over the target that is typical of energy transfer from impinging gas molecules.[22] The ANSYS finite element code was used for this transient thermal analysis. It was assumed that the target is not tumbling (i.e., the same side of the target is always facing forward, and the leading edge of the target is exposed to the maximum heat flux during the entire time of flight). Temperature-dependent D-T properties were used, and the latent heat of fusion was included to model the phase change.[22]

Figure 7 summarizes the results for a target injected at 400 m/s in the chamber. It shows the maximum change in the D-T temperature as a function of the maximum heat flux at the target surface for three different chamber radii (affecting the time of flight for a given injection velocity). The temperature rise of the target increases in a linear fashion up to the triple point of D-T, where a knee in the curve indicates that solid-to-liquid-phase change has occurred. From Fig. 7, the heat flux to reach the triple

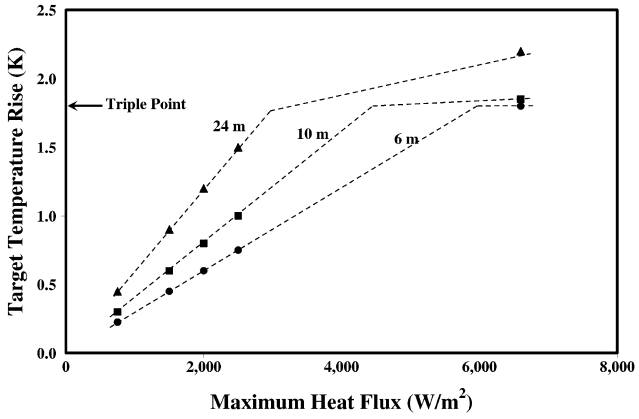

Fig. 7. Increase in the temperature of the 154-MJ direct-drive target during travel in the chamber as a function of the maximum incident heat flux (4-mm target at 18 K injected at 400 m/s) for three different chamber radii. The heat flux on the target varies along the target surface with the maximum heat flux occurring at the leading edge.

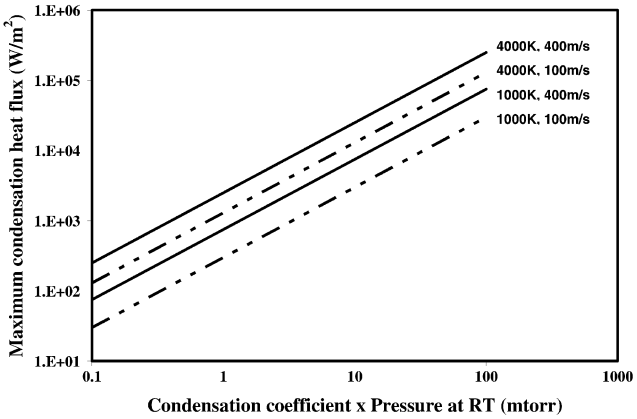

Fig. 8. Maximum condensation heat flux on the 154-MJ direct-drive target as a function of the product of $\{\sigma_c P_{Xe}(\text{at } 300\text{ K})\}$ for different values of xenon temperatures and injection velocities.

point is only ~6000 W/m^2 for a 6-m-radius chamber and even lower for larger chambers.

An estimate of the heat load on the target can be made by considering the combination of radiation heat flux from the wall and energy transfer from the chamber gas through which the target must travel (such as a buffer gas for dry-wall schemes). For example, a radiation heat flux of 6000 W/m^2 on the target is calculated for a wall temperature of 1275 K, assuming a reflectivity of ~96% that is anticipated for the very thin coating of gold (0.275 to 0.375 μm) on the target.[21] As the radiation heat flux scales as T^4, the radiation heat flux on the target can be reduced substantially at a lower wall temperature: For a wall temperature of 500°C, the radiation heat flux would be seven times smaller.

The transfer of energy from the impinging chamber gas (e.g., xenon or helium) would include both enthalpy exchange as the temperature of the impinging gas molecules is reduced to the target surface temperature as well as latent heat exchange in the case of gas condensation (i.e., if the background gas boiling and melting points are higher than the target temperature, as is the case with xenon). Figure 8 shows the maximum condensation heat flux as a function of the product of xenon pressure (at 300 K) P_{Xe} as well as the condensation coefficient σ_c, for different xenon temperatures and injection velocities. It is clear that for a reasonable wall temperature (~500°C), heating of the target is dominated by energy transfer from the chamber gas. As such, lower injection velocities are preferable. From Fig. 8, for a target velocity of 100 m/s, a heat flux of 6000 W/m^2 corresponds to example combinations of xenon temperature and pressure of 4000 K and 5 mtorr or 1000 K and ~20 mtorr (for $\sigma_c = 1$). This would place an important constraint on the background gas density as well as on the background gas temperature.

BUCKY simulations indicate that even 500 μs after target explosion, the average temperature of buffer gas in the chamber is ~2 eV. Previous studies had assumed that the buffer gas will cool down and achieve a temperature equilibrium with the chamber wall (~1000 K) in the interval between shots. Initial simulation of the chamber environment on a long timescale with the 2-D SPARTAN code[23] shows, however, that (a) because of reflection and convergence of initial shocks, the buffer gas in the central portion of the chamber can be heated to 40 eV and (b) thermal conduction to the wall is not strong enough to cool the buffer gas in the interval between shots (xenon gas temperature in the range of 5000 to 10 000 K at 100 ms after the target explosion). Much research is still needed to quantify the chamber condition (specifically buffer gas temperature) prior to initiation of a shot.

It should be noted that even if no buffer gas is introduced into the chamber, the chamber may contain significant amounts of deuterium and tritium (from the target) and helium (from fusion burn). These ions will be implanted into the wall, diffuse back into the chamber, and reach a steady-state condition depending on the pumping rate of the chamber. Most probably, the chamber environment will be enriched in helium as it is more difficult to pump helium compared to D-T with cryopumps. A similar analysis of target heating was performed with helium as the background gas to provide an estimate of acceptable helium pressure in the chamber. For conditions similar to those of Fig. 8, these simulations actually yielded slightly higher heat fluxes than for the case of xenon even though there is no helium phase change at the target surface temperature of 18 K. This can be explained as follows. First, the latent heats have only a small effect

on the overall energy transfer that is mostly governed by the change in the gas enthalpy. Second, the molecular fluxes of helium on the moving target are higher than those of xenon for the same pressure and temperature.[9] However, the condensation coefficient of helium might be substantially lower than that of xenon, which allows a much higher pressure in the chamber (or a lower heat flux for similar pressure). In addition, the equilibrium helium temperature between shots may be much lower than that of xenon because a lower amount of target energy would be absorbed in helium as opposed to xenon. Experimental data are needed in order to validate these models.

Clearly, increasing the target thermal robustness can substantially increase the maximum gas pressure allowed in the chamber. Possible ways of increasing this thermal robustness include target design modifications and extension of the D-T thermal limit by accepting phase change past the triple point. Initial results suggest that allowing ~1% change in the region density at the D-T foam–plastic coating interface would increase the allowable heat flux to 40 000 W/m^2 and adding a 72-μm-thick, 25%-dense outer insulating foam layer on the target would further increase the allowable heat flux to 90 000 W/m^2 (Ref. 22). Another possibility would be to develop techniques to lower the initial injection temperature of the target (below 18 K) while maintaining the required surface smoothness. It is not yet clear to which extent these particular measures are acceptable based on target physics requirements.

V.B. Target Tracking

Inertial fusion energy targets should be injected into an IFE chamber with sufficient velocity (50 to 400 m/s) and placed within ~2 to 5 mm of the chamber center (where driver beams are focused). For lasers, this requirement (5-mm variation) is due to the required symmetry of driver illumination of targets (translated into maximum variation in the arrival time of laser pulses from different beam lines on the target in an ~6-m-radius chamber). Within this 5-mm sphere, the laser steering system would focus the laser beams on the target within an accuracy of 20 μm (Sec. VI.A). Similar requirements have also been derived for heavy-ion-beam drivers (Sec. VI.B).

In addition to shot-to-shot variation caused by the operation of the injector itself, chamber gas eddies and/or a sufficient number of collisions with aerosol particles can cause the target trajectory to be deflected during its travel through the chamber. Obviously, the chamber environment should be returned to a sufficient quiescent condition prior to the initiation of the subsequent shot such that these random changes in target positioning are acceptably small (<5 mm). In-chamber tracking of the target is also necessary in order to (a) provide position information for the laser steering system and (b) provide long-term feedback for the target injector itself.

VI. BEAM TRANSPORT AND FOCUSING

VI.A. Lasers

VI.A.1. Transport and Focusing

Research in laser beam transport and focusing in IFE chambers is very limited as most present laser fusion experiments operate in vacuum. Many mechanisms may limit the density and type of chamber constituents. A well-known limit is laser breakdown of the background gases (or laser-generated spark). As the laser beam is focused, the electric field intensity may become large enough to induce a breakdown in the chamber gas. The laser light is then absorbed in the generated plasma or reflected back instead of reaching the target. If the laser photon energy matches transition energies in the background gas atoms, laser breakdown may be initiated even at smaller gas densities. Existence of a background plasma in the chamber may also lead to the initiation of laser breakdown at a lower gas pressure. Another limit derives from nonlinear changes in the index of refraction of the media (chamber gas) at high laser intensities that may distort the laser wave front at even lower gas densities. In this case, the laser beam may not focus on the target, and/or the variation of the laser intensity on the target may become unacceptably large. Large density and temperature gradients in the chamber gas can also deflect and/or defocus the laser light. At present, the only experimental data available for laser beam propagation and focusing in an inertial fusion chamber are from experiments in the NIKE facility.[24] In these experiments, drastic changes in the response of the planar targets were observed when the xenon pressure was raised above 100 mtorr (Ref. 24). Much more work is needed in this area to identify the proper limits for laser propagation and focusing in IFE chambers.

VI.A.2. Beam Steering

The focal spot of the laser beam should be adjustable within a few millimeters (less than $\pm$2.5 mm based on the requirement for uniform illumination of the target) with an accuracy of ~20 μm to compensate for inaccuracy of the target positioning. This can be accomplished by steering of the final focusing optics [e.g., grazing incident metal mirror (GIMM)]. Assuming that the final optics is placed 20 m from the center of the chamber, the final optics position (i.e., the angle with respect to the incoming beam) should be controlled with an accuracy of 1 μrad and a range of 100 μrads. One approach would be to mount the final optics on piezoelectric actuators. Assuming that the GIMM is made of 50- $\times$ 50-cm square segments, steering of the laser beam requires actuators with an accuracy of 0.5 μm and a range of 50 μm operating at 1 kHz or less, which is well within the capability of these actuators.

VI.B. Heavy Ions

VI.B.1. Transport and Focusing

For a heavy-ion driver, the requirements posed on the chamber gas depend on the mode of transport and focusing.[25] Various transport modes for heavy-ion beams are listed in Table III. Most present R&D is focused on the neutralized ballistic transport mode. As part of the ARIES-IFE study, extensive studies of pinch transport modes were performed.[6] These studies have not uncovered any feasibility issues for these modes of transport. If the predictions for these transport modes are verified experimentally in power plant–class driver conditions, they would lead to dramatic improvements in heavy-ion fusion systems.

Several processes affect transport of heavy-ion beams in the chamber. These include (for both gas and aerosols) the following:

1. energy loss through interaction of beam particles with chamber constituents (i.e., classical stopping power). A limit of 10% energy loss was used here.
2. scattering of beam through interaction with chamber constituents. Assuming emittance dominated spots, a limit of 10% increase in the spot area (5% increase in radius) was used here.
3. stripping of beam ions that may prevent focusing.

For neutralized ballistic transport, stripping is the dominant limit. Stripping depends on the total amount of matter in the path of the beam (either gas or aerosol). For a chamber with flibe as the protective coolant, LSP simulations[6] lead to the flibe aerosol constraint of $nr^3 \leq 10^{-9}$ (no gas) or a 1-mtorr limit for the flibe base pressure in a 3-m-radius chamber (no aerosol). These constraints can be easily extended to chambers with both gas and aerosol. In the above, n is density of aerosol droplets, and r is the radius of the aerosol. Scattering is the dominant mechanism for assisted pinch transport. This mode of transport is more forgiving and has a higher limit of $nr^3 \leq 10^{-6}$ for aerosol (no gas) or ~1 Torr of gas (no aerosol). For self-pinch transport, the self-pinching process itself is the most stringent requirement and leads to $nr^3 \leq 10^{-7}$ for aerosols (no gas) or ~100 mtorr of gas (no aerosol). These constraints on nr^3 or base vapor pressure can be easily extrapolated to different chamber sizes (nr^3 scales inversely with the chamber radius) and protective liquid type (see correlations in Ref. 25).

VI.B.2. Beam Steering

The focal spot of the beam should be adjustable within a few millimeters (less than ±2 mm) to compensate for inaccuracy of the target within ~10 ms. This can be accomplished by dipole correctors in the final focus.[26] The requirements for this correction dipole (~1 kG in ~10 ms) are lower than the correction coils for shot-to-shot correction in present experiments (~7 kG in 1 ms in the Neutralized Transport Experiment).

TABLE III

A Comparison of Heavy-Ion Transport and Focusing Modes and Constraints Imposed by the Presence of Gas and/or Aerosol in the Chamber*

Transport Mode	Constraints
Vacuum ballistic	Not considered (requires ≤0.1 mtorr background pressure)
Neutralized ballistic	A preformed plasma is produced. <1 mtorr for ~3-m radius, ~50 to 200 beams[a] Aerosol constraint: $nr^3 \leq 10^{-9}$
Assisted pinch	A preformed channel is produced using laser and *Z*-pinch discharges. 1 to 10 torr, two beams Aerosol constraint: $nr^3 \leq 10^{-6}$
Self-pinched	1 to 100 mtorr, ~2 to 100 beams Aerosol constraint: $nr^3 \leq 10^{-7}$

*Constraints are given in terms of n (aerosol integrated line density) and r (radius of aerosol) for 4-GeV lead beam. Constraints are given for cases of aerosol parameters (and no gas) and gas number density (and no aerosol).

[a]The increase in chamber radius for dry- and wetted-wall concepts leads to even more stringent constraints on vacuum and beam emittance compared to thick-liquid wall.

VII. OPERATIONAL WINDOWS FOR DRY-WALL CHAMBER CONCEPTS

VII.A. Direct-Drive Targets

Operational windows for IFE chambers can be evolved by superimposing the constraints imposed by each system as described in Secs. III, V, and VI. For dry-wall chambers with direct-drive targets, the majority of these constraints depends on the the buffer gas pressure and the chamber armor equilibrium temperature allowing a compact representation. For example, Fig. 9 shows an operational window for chamber gas pressure and wall temperature (for a 6.5-m-radius chamber with carbon armor and xenon as protective gas for the 154-MJ direct-drive target). The original armor thermal operational window is significantly reduced when the laser breakdown constraint, limiting the xenon pressure to <100 mtorr, is taken into account. The operational window is further reduced even assuming an optimistic constraint of 20 mtorr/1000 K xenon based on target survival (unhashed region in Fig. 9). The operational window for the

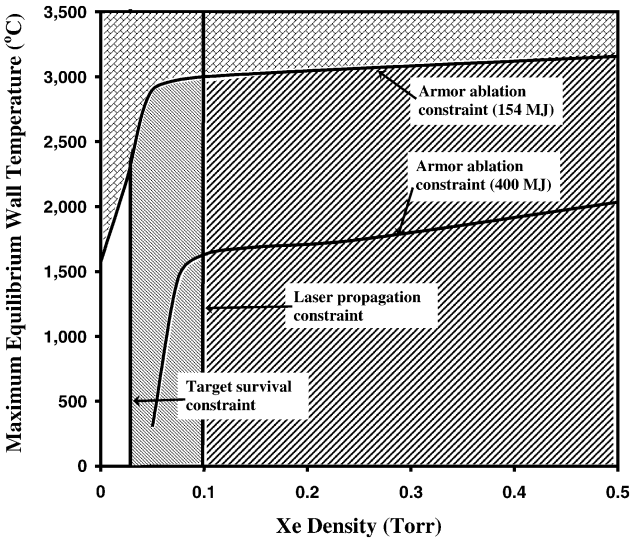

Fig. 9. Operational window (unhashed region) for buffer gas density and wall temperature of dry-wall chambers with direct-drive targets (6.5-m-radius chamber with carbon armor). For a relatively low yield target (<250 MJ), no buffer gas is necessary, and an operation window exists (see discussion in the text).

case of chambers with a tungsten armor is similar to Fig. 9.

Based on the constraint developed in Secs. III, V, and VI, the following observations can be made about the operational windows for dry-wall chambers with direct-drive targets:

1. The most stringent constraint is imposed by target survival during the injection process. Operation with a reasonable wall temperature (~500°C) minimizes the radiation heating of the target as well as allows for acceptable thermal conversion efficiency. Low target velocity (100 m/s) is preferable. There are strict constraints on the pressure and temperature of the buffer gas. Experiments of target heating by high-temperature xenon and helium is necessary to validate these calculations. The major unknowns are the condensation coefficients.

2. There are indications that the xenon buffer gas will not cool down sufficiently between shots.[23] Investigation of chamber evolution between shots is necessary to develop a more accurate representation of the chamber condition prior to each shot and to gain confidence in the estimates for target heating during the injection process.

3. For relatively low yield targets (<250 MJ), an operational window with no buffer gas may exist (based on the above lifetime criterion). The chamber gas constituents would be mainly deuterium, tritium, and helium (from the target), and their density must be kept low by providing sufficient pumping.

4. Very few data are available on the operational window for propagation and focusing of laser beams in IFE chamber gas constituents.

5. The armor lifetime could be further limited by other mechanisms, such as the long-term response of the armor to the cycle heat load as well as armor damage due to high-energy ions (especially exfoliation by high-energy helium). These are major concerns that need to be investigated through R&D.

6. Development of a more thermally robust target to increase the size of the operational window is needed. This would allow for higher-yield targets and would help accommodate other possibly more restraining armor lifetime criteria as well as the possibility of higher heat fluxes on the target as it traverses the chamber.

We have not considered heavy-ion-beam transport and focusing constraint for chamber concepts with direct-drive targets because of the difficulties associated with heavy-ion-beam drivers in a direct-drive configuration (large sections for bending the beam and many final focus elements).

VII.B. Indirect-Drive Targets

An overall operational window for dry-wall chambers with indirect-drive targets can be similarly developed. Because the IFE capsule is protected by the relatively massive hohlraum during the injection and passage through the chamber, there is virtually no target heating constraint. The operational window depends on the thermal response of the wall, lifetime of the armor, and driver beam propagation and focusing.

For 458-MJ indirect-drive targets, the buffer gas should have a density of >200 mtorr (see Fig. 5). This minimum value is a factor of 2 higher than the relatively uncertain constraint of <100 mtorr xenon density for laser propagation, which implies that no window exists for KrF laser drivers. Further R&D on laser propagation and focusing is needed to resolve this issue.

For the heavy-ion-beam driver, the existence of an operational window would depend on the mode of transport. There is no operational window based on requirements from neutralized ballistic transport (stripping limit of integrated line gas density equivalent to ~1 mtorr versus minimum buffer gas pressure of 200 mtorr). It appears that no operation window exists for self-pinched transport (integrated line density equivalent to ~100 mtorr versus a minimum buffer gas pressure of 200 mtorr). Further research is necessary to refine the beam transport constraint in this mode before completely ruling out this approach. A large operational window, however, exists for channel transport (scattering limit of integrated line density equivalent to ~1 torr). Experimental verification of channel transport is needed to confirm this conclusion.

A generic issue for concepts with indirect-drive targets is the large amount of hohlraum material that is introduced into the chamber and should be removed continuously. This is an especially major concern for dry-wall chamber concepts. Further theoretical and experiment research in IFE chamber clearing is needed.

VIII. OPERATIONAL WINDOWS FOR WETTED-WALL CHAMBER CONCEPTS

The issue of generation and transport of aerosols in the chamber is key to arriving at an acceptable operational window for the injection of targets and propagation of driver beams as is discussed below.

Aerosol droplets can condense on the direct-drive targets during their transit through the chamber. In addition to heating the target, the added material on the target may change the ignition characteristics of the targets. Detailed target physics analysis is necessary to develop limits on aerosol condensation on direct-drive targets. In addition, data do not exist for propagation of laser beams in aerosol-filled chambers. Therefore, we did not investigate the wetted-wall chamber with direct-drive targets in detail.

Results from the aerosol analysis described in Sec. IV and discussed in detail in Ref. 4 can be used to evolve an operational window for a wetted-wall configuration with indirect-drive targets and heavy-ion drivers. For example, Fig. 10 shows the vapor and aerosol mass histories for a 6.5-m-radius chamber with a flibe wetted wall exposed to the photon threat spectrum of the 458-MJ indirect-drive target. Heating from ions that arrive later in time was not considered for this estimation. The aerosol mass for the 6.5-m-radius-chamber case increases to ~3.5 kg within a few milliseconds and stays roughly constant thereafter as no wall coagulation (possible sink term) is assumed. The vapor pressure decreases continuously because of condensation on the wall. The aerosol mass of 3.5 kg corresponds to $nr^3 = 5 \times 10^{-7}$ and should be compared to values given in Table III. Clearly, the remaining flibe mass in the chamber is much above the stripping limit for neutralized ballistic transport and a factor of 5 above the self-pinched transport limit of 100 mtorr, which leaves only channel transport as a possible mode of ion beam transport.

The aerosol behavior is dependent on a number of parameters such as the aerosol source term, the size of the chamber, and the wetted-wall fluid. For example, reducing the size of the chamber for the given target yield results in a higher energy deposition intensity from the photons and in a higher ablation depth of the wetted wall. Figure 11 shows the vapor and aerosol mass histories for a 3-m-radius chamber with a flibe wetted wall exposed to the photon threat spectrum of the 458-MJ indirect-drive target.[4] The ablation source term in this case corresponds to ~11.5 μm of flibe as opposed to 5.5 μm for the 6.5-m-radius-chamber case. As shown in Fig. 11, the aerosol mass in the chamber reaches a value (1.8 kg) that is actually lower than for the 6-m-radius-chamber case; however, the aerosol density in the chamber is much higher ($nr^3 = 8 \times 10^{-6}$) and would preclude any heavy-ion transport mode. Even the vapor pressure by itself (~100 mtorr after 0.2 s) would preclude the neutralized ballistic transport mode but would allow the self-pinched and channel transport modes.

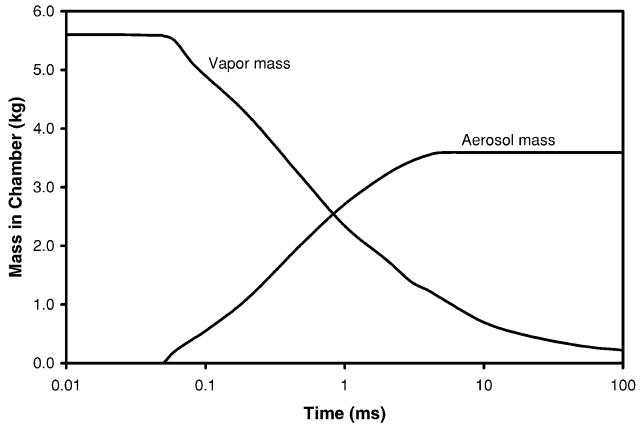

Fig. 10. Vapor and aerosol mass histories for a 6.5-m-radius chamber with a flibe wetted wall exposed to the photon threat spectrum of the indirect-drive target (assuming an ablated thickness of 5.5 μm). The aerosol mass of 3.5 kg corresponds to $nr^3 = 5 \times 10^{-7}$ and is 500 times larger than the limit for neutralized ballistic transport and 5 times larger than self-pinched transport (see Table III).

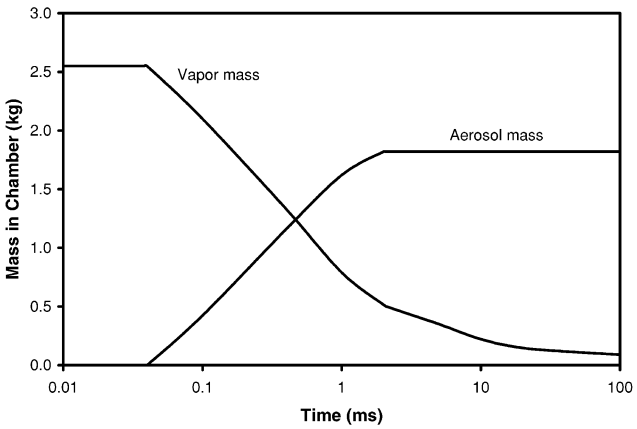

Fig. 11. Vapor and aerosol mass histories for a 3-m-radius chamber with a flibe wetted wall exposed to the photon threat spectrum of the indirect-drive target (assuming an ablated thickness of 11.5 μm). While the total aerosol mass in the chamber (1.8 kg) is lower than for the 6-m-radius-chamber case (Fig. 10), the aerosol density in the chamber is much higher ($nr^3 = 8 \times 10^{-6}$).

There are many uncertainties in the analysis of aerosol generation and transport in the IFE chambers such as the coagulation and reflection behavior of droplets of different sizes and velocities impacting a liquid wall (aerosol transport) as well as ion-enhanced nucleation (aerosol generation). Droplets entering the chamber through explosive boiling should also be considered. Aerosol generation and transport is also a critical feasibility issue for thick-liquid-wall chambers. These issues need to be further addressed through a coordinated experimental and modeling R&D effort.

IX. SUMMARY AND CONCLUSIONS

As part of the ARIES-IFE study, we have performed detailed analysis of various subsystems parametrically to uncover key physics and technology uncertainties and to identify constraints imposed by each subsystem on the feasibility of IFE chamber concepts.[3–8] In this paper, the constraints from various subsystems were combined in order to understand the trade-offs among subsystems, to develop operational windows for IFE chamber concepts, and to identify high-leverage R&D directions for IFE research.

We selected a heavy-ion indirect-drive target design from LLNL/LBL and a direct-drive target design from NRL as our reference targets. Detailed spectra from these two targets have been calculated—their photon and ions/debris spectra are vastly different. We have shown that the detailed characterization of the target yield and spectrum has a major impact on the response of the chamber.

Dry-wall chambers are desirable because of their relative simplicity. The energy threat to the first wall by high-energy ions and X rays falls by one to two orders of magnitude within the first 100 μm of the first wall. As such, it is prudent to use a thin armor instead of a monolithic first wall. Armor can then be optimized to handle rapid particle and heat fluxes while the first wall is optimized for structural function and efficient heat removal at quasi steady state. IFE armor conditions are similar to those for plasma-facing components in MFE devices as is shown in Table II. As such, the large body of research performed for MFE plasma-facing components is directly applicable to IFE armors. Furthermore, as most of the neutrons are deposited in the back where the blanket and coolant temperature will be at quasi steady state because of the thermal capacity effect, most first-wall and blanket concepts developed for MFE will be directly applicable to IFE applications.

For dry-wall concepts with direct-drive targets, we have found that the most stringent constraint is imposed by target survival during the injection process. Operation with a reasonable wall temperature ($\sim$500°C) minimizes the radiation heating of the target as well as allows for acceptable thermal conversion efficiency. There are strict constraints on the pressure and temperature of the buffer gas. For relatively low yield targets ($<$250 MJ), an operational window with no buffer gas may exist (based on armor survival criteria of no ablation for carbon and no melting for tungsten). The chamber gas constituents would be mainly deuterium, tritium, and helium (from the target), and their density must be kept low by providing sufficient pumping. However, the armor lifetime could be further limited by other mechanisms, such as the long-term response of the armor to the cycle heat load as well as armor damage due to high-energy ions (especially exfoliation by high energy helium).

For dry-wall concepts with indirect-drive targets, a high buffer gas pressure would be necessary. This may preclude propagation of the laser driver in the chamber and may require assisted pinch transport for the heavy-ion driver. A generic issue for concepts with indirect-drive targets is the large amount of hohlraum material that is introduced into the chamber and that should be removed continuously.

The wetted- or thin-liquid-protected wall concept combines the attractive features of a solid wall (robust mechanical design and efficient energy recovery) with the advantages of a renewable armor to accommodate the X-ray and ion threat produced by IFE target explosions. Renewability of the liquid-film armor removes the near-zero ablation threshold of a solid wall armor. On the other hand, part of the liquid-film armor evaporates under the incident X-ray and ion energy fluxes and enters the chamber in each shot. The key feasibility issues for the wetted-wall concept are (a) reestablishment of the liquid-film armor between shots and (b) reestablishment of a sufficiently quiescent chamber environment prior to the next shot. Reestablishment of the liquid protection film by radial injection through a porous wall appears to be feasible and does not impose major constraints on the feasibility of wetted-wall concepts. The attractiveness of this scheme, to a large degree, depends on the details of the chamber and power plant design and the impact of the required pumping power on the overall recirculating power and economics of the power plant. For the forced-flow scheme, the behavior of the film near major obstacles is a major concern and requires further R&D.

The generation and transport of aerosols in the chamber is a key issue in arriving at an acceptable operational window for the injection of targets and propagation of driver beams. Our initial estimates indicate that a substantial amount of liquid protection film will remain in the chamber as aerosol. Survival of a direct-drive target during the injection process as well as propagation of laser beams in such an environment are major concerns. For indirect-drive targets and heavy-ion drive, the assisted pinch transport mode is necessary. There are many uncertainties in the analysis of aerosol generation and transport in the IFE chambers such as the coagulation and reflection behavior of droplets of different sizes and velocities impacting a liquid wall (aerosol transport) as

well as ion-enhanced nucleation (aerosol generation). Droplets entering the chamber through explosive boiling should also be considered. Aerosol generation and transport are also a critical feasibility issue for thick-liquid-wall chambers. These issues need to be further addressed through a coordinated experimental and modeling R&D effort.

ACKNOWLEDGMENT

This work was supported by the U.S. Department of Energy under contract DE-FC03-95ER54299.

REFERENCES

1. I. N. SVIATOSLAVSKY et al., "A KrF Laser Driven Inertial Fusion Reactor SOMBRERO," *Fusion Technol.*, **21**, 1470 (1992); see also W. R. MEIER et al., "OSIRIS and SOMBRERO Inertial Fusion Power Plant Designs: Final Report," Schaffer Associate report WJSA-92-01 (also DOE/ER/54100-1) (1992).

2. L. M. WAGANER et al., "Inertial Fusion Energy Reactor Design Studies, PROMETHEUS-L, PROMETHEUS-H—Final Report," MDC92E0008, McDonnell Douglas Aerospace (also DOE/ER-54101) (1992).

3. A. R. RAFFRAY, L. EL-GUEBALY, G. FEDERICI, D. HAYNES, F. NAJMABADI, D. PETTI, and ARIES-IFE TEAM, "Dry-Wall Survival Under IFE Conditions," *Fusion Sci. Technol.*, **46**, 417 (2004).

4. A. R. RAFFRAY, S. I. ABDEL-KHALIK, D. HAYNES, F. NAJMABADI, P. SHARPE, M. YODA, M. ZAGHLOUL, and ARIES-IFE TEAM, "Thermo Fluid Dynamics and Chamber Aerosol Behavior for Thin Liquid Wall Under IFE Cyclic Operation," *Fusion Sci. Technol.*, **46**, 438 (2004).

5. M. YODA, S. I. ABDEL-KHALIK, and ARIES-IFE TEAM, "An Investigation of the Fluid Dynamics Aspects of Thin Liquid Film Protection Schemes for Inertial Fusion Energy Reactor Chambers," *Fusion Sci. Technol.*, **46**, 451 (2004).

6. D. V. ROSE, D. R. WELCH, C. L. OLSON, S. S. YU, S. NEFF, W. M. SHARP, and ARIES-IFE TEAM, "Impact of Beam Transport Method on Chamber and Driver Design for Heavy Ion Inertial Fusion Energy," *Fusion Sci. Technol.*, **46**, 470 (2004).

7. L. BROMBERG and ARIES-IFE TEAM, "Design Requirements and Options for Final Focusing Superconducting Magnets of Heavy-Ion Drivers," *Fusion Sci. Technol.*, **46**, 494 (2004).

8. L. EL-GUEBALY, P. WILSON, D. HENDERSON, A. VARUTTAMASENI, and ARIES-IFE TEAM, "Feasibility of Target Material Recycling as Waste Management Alternative," *Fusion Sci. Technol.*, **46**, 506 (2004).

9. D. A. CALLAHAN-MILLER and M. TABAK, "Increasing the Coupling Efficiency in a Heavy Ion, Inertial Confinement Fusion Target," *Nucl. Fusion*, **39**, 1547 (1999).

10. S. E. BODNER, D. G. COLOMBANT, A. J. SCHMITT, and M. KLAPISCH, "High-Gain Direct-Drive Target Design for Laser Fusion," *Phys. Plasmas*, **7**, *6*, 2298 (2000).

11. "ARIES-IFE Reference Target Spectra," available on the Internet at ⟨http://aries.ucsd.edu/ARIES/DOCS/ARIES-IFE/SPECTRA⟩.

12. R. W. CONN et al., "Solase, A Conceptual Laser Fusion Reactor Design," UWFDM-220, University of Wisconsin, Madison (Dec. 1977).

13. F. NAJMABADI et al., "Assessment of Chamber Concepts for Inertial Fusion Energy Power Plants—The ARIES-IFE Study," *Proc. Int. Symp. Inertial Fusion Science and Applications (IFSA 2001)*, Kyoto, Japan, September 2001, p. 701, Elsevier Data Science Library (2001); see also F. NAJMABADI, "Laser-Driven IFE Power Plants—Initial Results from ARIES-IFE Study," *Proc. 3rd U.S./Japan Workshop Laser-Driven Inertial Fusion Energy*, Livermore, California, January 25–27, 2001.

14. Y. KOZAKI et al., "Issue and Design Windows of Laser Fusion Reactor Chambers," *Proc. 19th IAEA Fusion Energy Conf.*, Lyon, France, 2002, IAEA/CN-94/FTP1/25, International Atomic Energy Agency.

15. J. J. MacFARLANE et al., "BUCKY-1, A 1-D Radiation Hydrodynamics Code For Simulating Inertial Confinement Fusion High Energy Density Plasmas," UWFDM-984, University of Wisconsin (1995); see also R. R. PETERSON et al., "The BUCKY and ZEUS-2D Computer Codes for Simulating High Energy Density ICF Plasmas," *Fusion Technol.*, **30**, 783 (1996).

16. S. SHIN, S. I. ABDEL-KHALIK, D. JURIC, M. YODA, and ARIES TEAM, "Effects of Surface Evaporation and Condensation on the Dynamics of Thin Liquid Films for the Porous Wetted Wall Protection Scheme in IFE Reactors," *Fusion Sci. Technol.*, **44**, 117 (2003).

17. J. K. ANDERSON, S. G. DURBIN II, M. YODA, D. L. SADOWSKI, M. YODA, S. I. ABDEL-KHALIK, and ARIES TEAM, "Experimental Studies of High-Speed Liquid Films on Downward-Facing Surfaces for Inertial Fusion Energy Wet Wall Concepts," *Fusion Sci. Technol.*, **43**, 401 (2003).

18. D. T. GOODIN et al., "A Credible Pathway for Heavy Ion Driven Target Fabrication and Injection," *Laser Particle Beams*, **20** (2002).

19. D. T. GOODIN et al., "Addressing the Issues of Target Fabrication and Injection for Inertial Fusion Energy," *Fusion Eng. Des.*, **69**, 803 (2003).

20. D. T. GOODIN, N. B. ALEXANDER, C. R. GIBSON, A. NOBILE, R. W. PETZOLDT, N. P. SIEGEL, and L. THOMSON, "Developing Target Injection and Tracking for Inertial Fusion Energy Power Plants," *Nucl. Fusion*, **41**, 527 (2001).

21. R. W. PETZOLDT et al., "Direct Drive Target Survival During Injection in an Inertial Fusion Energy Power Plant," *Nucl. Fusion*, **42**, 1351 (2002).

22. A. R. RAFFRAY, R. PETZOLDT, J. PULSIFER, M. S. TILLACK, and X. WANG, "Thermal Behavior and Operating Requirements of IFE Direct-Drive Target," *Fusion Sci. Technol.*, **44**, 111 (2003).

23. Z. DRAGOJLOVIC and F. NAJMABADI, "Simulation of IFE Chamber Dynamics Response by a Second Order Godunov Method with Arbitrary Geometry," *Proc. Int. Symp. Inertial Fusion Science and Applications (IFSA 2003)*, Monterey, California, September 2002, Elsevier Data Science Library (2003).

24. J. SETHIAN, Naval Research Laboratory, Personal Communication (2002).

25. C. OLSON, "Beam Chamber Transport Requirements for FLiBe Vapor Pressure and Aerosol Conditions," presented at ARIES Program Meeting, October 2002, available on the Internet at ⟨http://aries.ucsd.edu/ARIES/MEETINGS/0210/⟩.

26. S. YU, "Beam Steering Capability for Target Position Uncertainty," presented at ARIES Program Meeting, October 2002, available on the Internet at ⟨http://aries.ucsd.edu/ARIES/MEETINGS/0210/⟩.